Inorganica Chimica Acta 362 (2009) 3657–3662

Contents lists available at ScienceDirect

Inorganica Chimica Acta

journal homepage: www.elsevier.com/locate/ica

Synthesis, crystal structure and magnetic characterization of two new ion-pair complexes containing bis(maleonitriledithiolate)nickelate anion and substituted benzylpyridinium cation

Hong-Rong Zuo [a], Li-Xia Wu [a], Qian Huang [a], Xing Chen [a], Jia-Rong Zhou [a], Le-Min Yang [a], Chun-Lin Ni [a,*], Xue-Lei Hu [b]

[a] Department of Applied Chemistry, Centre of Inorganic Functional Materials, College of Science, South China Agricultural University, Wushan, Tianhe District, Guangzhou, Guangdong 510642, PR China
[b] School of Chemical Engineering and Pharmacy, Wuhan Institute of Technology, 430073 Wuhan, PR China

ARTICLE INFO

Article history:
Received 2 December 2008
Received in revised form 4 April 2009
Accepted 17 April 2009
Available online 3 May 2009

Keywords:
Substituted 4-dimethylaminopyridinium
Bis(maleonitriledithiolate)nickelate
Crystal structure
Magnetic properties
Spin-gap transition

ABSTRACT

Two new ion-pair complexes, $[FBrBzPyN(CH_3)_2]_2[Ni(mnt)_2]$ (**1**) and $[FBrBzPyN(CH_3)_2][Ni(mnt)_2]$ (**2**) (mnt^{2-} = maleonitriledithiolate, $[FBrBzPyN(CH_3)_2]^+$ = [1-(4′-fluoro-2′-bromobenzyl)-4-dimethylamino-pyridinium]) have been prepared and characterized by elemental analyses, UV, IR, single crystal X-ray diffraction and magnetic susceptibility. The cations (D) and the anions (A) in **1** stack into a 1D alternating column (i.e., of type ···DDADDADD···) *via* short S···Br, N···F, C···N interactions, and C–H···Br hydrogen bonds. The cation–cation π···π stacking interactions within the columns give further rise to a 2D network structure. Compound **2** forms a 3D structure in which the Ni(III) ions stack into a uniform 1D zigzag magnetic chain through Ni···S, Ni···Ni, or π···π interactions with a Ni···Ni distance of 4.024 Å. Magnetic susceptibility measurements in the temperature range 2–300 K show that **1** is expected to be diamagnetic, and **2** exhibits an interesting spin-gap transition (Δ/k_b = 460.6 K) around 155 K.

1. Introduction

The syntheses and properties of numerous molecular magnets that possess spin bistability have received attention in recent years due to their potential applications in molecular switch, data storage and displays [1–4]. In this regard, the spin molecular system based on $[M(mnt)_2]^-$ (M = Ni, Pd, or Pt ions, mnt^{2-} = maleonitriledithiolate) anions are very attractive in that it posses a planar configuration with an extended electronic structure and the magnetic coupling is highly sensitive to the interactions contacts and the overlap patterns of $[M(mnt)_2]^-$ anions [5–10]. As a part of our continuing efforts to find more suitable counter ions to tune the crystal stacking structure of $[M(mnt)_2]^-$ anions with a view to obtaining ideal magnetic materials displaying a spin gap transition [11–13]. In this direction, we have recently utilized substituted 4-dimethylaminopyridinium as countercations to obtain three new ion-pair complexes, $[BiClBzPyN(CH_3)_2][Ni(mnt)_2]$ [14], $[BrFBzPyN(CH_3)_2][Ni(mnt)_2]$ [15] and $[FClBzPyN(CH_3)_2][Ni(mnt)_2]$ [16], in which the $[Ni(mnt)_2]^-$ anions and the cations stack into well-segregated columns and the Ni(III) ions form a 1D zigzag chain through intermolecular Ni···S, S···S, Ni···Ni, or π···π interactions. It is interesting that these ion-pair complexes exhibit an unusual spin gap transition around 140 K, 200 K, and 55 K, respectively. With a view to extending our research work and investigating the effect of substituted groups in the phenyl ring of the cation on the structure and magnetic properties, two new ion-pair complexes, $[FBrBzPyN(CH_3)_2]_2[Ni(mnt)_2]$(**1**) and $[FBrBzPyN(CH_3)_2][Ni(mnt)_2]$(**2**), were designed and prepared to gain more insight into the magneto-structural relationship. The experimental results have shown that **1** and **2** form a 2D and 3D structure, respectively. The Ni(III) ions of **2** form a uniform 1D zigzag magnetic chain within a $[Ni(mnt)_2]^-$ column and the magnetic behavior is in agreement with a spin gap feature.

2. Experimental

2.1. General materials

All regents used in the syntheses were of analytical grade. 1-(4′-fluoro-2′-bromobenzyl)-4-dimethylaminopyridinium bromide ($[FBrBzPyN(CH_3)_2]Br$) and disodium maleonitriledithiolate (Na_2mnt) were synthesized following the literature procedures [17,18]. Elemental analyses were run on a Model 240 Perkin-Elmer CHN instrument. IR spectra were recorded on a Nicolet Avatar 360 FT–IR (4000–400 cm^{-1} region) spectrophotometer in KBr pellets.

---

* Corresponding author. Tel.: +86 20 85282568; fax: +86 20 85282366.
E-mail address: niclchem@scau.edu.cn (C.-L. Ni).

0020-1693/$ - see front matter © 2009 Elsevier B.V. All rights reserved.
doi:10.1016/j.ica.2009.04.021

Electronic spectra were recorded on a SHIMADZU UV-2550 spectrophotometer. All solution concentrations were *ca.* 10^{-5} mol dm^{-3} in CH_3CN. Magnetic susceptibility measurements were carried out in the temperature range 2–300 K using a Quantum Design MPMS-XL superconducting quantum interference device (SQUID) magnetometer.

2.2. Synthesis of $[FBrBzPyN(CH_3)_2]_2[Ni(mnt)_2])$(**1**)

To a solution of Na_2mnt (360 mg, 2 mmol) in water (20 cm^3), a solution of $NiCl_2{\cdot}6H_2O$ (238 mg, 1 mmol) in 10 cm^3 water was then added dropwise with vigorous stirring at room temperature. A solution of $[FBrBzPyN(CH_3)_2]Br$ (790 mg, 2 mmol) in 20 cm^3 MeOH was slowly added to the red solution above. The product was filtered, washed by water, dried under vacuum and recrystallized with acetone–MeOH to give red solid 817 mg, yield 85%. Elemental *Anal.* Calc. for $C_{36}H_{30}Br_2F_2N_8NiS_4$: C, 45.06; H, 3.15; N, 11.68. Found: C, 45.01; H, 3.23; N, 11.62%. IR (KBr, cm^{-1}): 3067(m), 2919(w), 2853(w), 2213(s), 2195(s), 1647(s), 1596(m), 1572(s), 1485(vs), 1451(m), 1227(s), 1163(s), 1148(s), 1107(m), 1035(s), 824(m), 807(m), 783(s), 737(m), 586(s), 538(s), 509(s).

2.3. Synthesis of $[FBrBzPyN(CH_3)_2][Ni(mnt)_2])$(**2**)

An acetone solution (10 cm^3) of I_2 (120 mg, 0.47 mmol) was slowly added to a acetone solution (20 cm^3) of **1** (721 mg, 0.75 mmol) and the mixture was stirred for 12 h. MeOH (60 cm^3) was then added, and the mixture allowed to stand overnight, 390 mg of black micro-crystals formed were filtered off, washed with MeOH and dried in vacuum. Yield: 80%. *Anal.* Calc. for $C_{22}H_{15}BrFN_6NiS_4$: C, 40.70; H, 2.33; N, 12.94. Found: C, 40.66; H, 2.38; N, 12.91%. IR (KBr, cm^{-1}): 3030(w), 2919(m), 2846(m), 2362(m), 2208(s), 1655(s), 1577(m), 1487(s), 1396(s), 1299(m), 1220(s), 1098(m), 987(m), 937(w), 876(s), 811(m), 533(m).

Single crystals suitable for X-ray structure analyses were obtained by evaporation of the solvents from MeCN/*i*-PrOH (v:v = 1:2) solutions of **1** and **2**.

2.4. Determination of crystal structure

X-ray diffraction experiments were performed with a Bruker SMART CCD area detector diffractometer using graphite monochromated Mo K*a* radiation ($\lambda = 0.71073$ Å) in ω and ϕ scans mode. A semi empirical absorption correction was carried out using SADABS [19]. Data collection, cell refinement and data reduction were done with the SMART and SAINT programs [20]. The structures were solved by direct method using SHELXS 2000 and refined on F^2 by full-matrix least-squares methods (SHELXL2000) [21]. All the non-hydrogen atoms were easily found from Fourier maps and refined anisotropically. Hydrogen atoms were constrained to ride on the respective carbon atoms with an isotropic displacement parameter equal to 1.2 times the equivalent isotropic displacement parameter of their parent atom. The details of data collection, refinement and crystallographic data are summarized in Table 1. Selected bond distances and angles are given in Table 2.

Table 1
Crystallographic data for **1** and **2.**

Compound	1	2
Empirical formula	$C_{36}H_{30}Br_2F_2N_8NiS_4$	$C_{22}H_{15}BrFN_6NiS_4$
Formula weight	959.45	649.26
Temperature/K	291(2)	291(2)
Crystal system	Triclinic	Monoclinic
Space group	$P\bar{1}$	$P2_1/c$
Unit cell dimensions		
a/Å	8.593(4)	7.0584(9)
b/Å	9.221(4)	17.869(2)
c/Å	13.507(6)	21.021(3)
α/°	77.932(5)	90
β/°	86.618(6)	92.063(2)
γ/°	72.054(5)	90
V/Å^3	995.7(8)	2649.6(6)
Z	1	4
Density (calculated), mg/m^3	1.600	1.628
Mu(Mo Kα)/mm	2.751	2.586
F(0 0 0)	482	1300
Crystal size/mm^3	0.12 × 0.18 × 0.25	0.11 × 0.13 × 0.25
θ_{min}, θ_{max} (°)	2.4, 25.0	1.9, 25.0
Reflection collected	6984	18650
Independent reflections (R_{int})	3450 (0.025)	4664 (0.031)
Data/restrains/parameters	6984/3450/243	18650/4664/318
Goodness of fit on F^2	1.046	1.017
Final R indices [$I > 2\sigma(I)$]	$R_1 = 0.0493$, $wR_2 = 0.1371$	$R_1 = 0.0510$, $wR_2 = 0.1862$
Final R indices (all data)	$R_1 = 0.0603$, $wR_2 = 0.1472$	$R_1 = 0.0697$, $wR_2 = 0.1982$
Largest difference peak and hole (e Å^{-3})	0.94 and −1.25	0.73 and −0.60

$R_1 = \Sigma(||F_o|-|F_c||)/\Sigma|F_o|$, $wR_2 = [\Sigma\ w(|F_o|2-|F_c|^2)^2/\Sigma\ w(|F_o|^2)^2]^{1/2}$.

Table 2
Selected bond parameters and intermolecular contacts for **1** and **2.**

Compound **1**			
Ni(1)–S(1)	2.1795(15)	S(1)–Ni(1)–S(2)	91.98(4)
Ni(1)–S(2)	2.1746(16)		
Compound **2**			
Ni(1)–S(1)	2.1450(16)	S(1)–Ni(1)–S(2)	92.06(7)
Ni(1)–S(2)	2.1502(19)	S(1)–Ni(1)–S(4)	87.82(7)
Ni(1)–S(3)	2.1484(16)	S(2)–Ni(1)–S(3)	87.82(6)
Ni(1)–S(4)	2.1434(19)	S(3)–Ni(1)–S(4)	92.33(7)

3. Results and discussion

3.1. Descriptions of structures

The structure of **1** composed of a cation and a half anion in an asymmetric unit is shown in Fig. 1a, and the anion lies on a centre of inversion. The NiS_4 core exists in the square planar coordination geometry. The bond lengths and angles within the anion are in fair agreement with those of other molecular solids based on $[Ni(mnt)_2]^{2-}$ anion and substituted pyridinium [22,23]. In the $[FBrBzPyN(CH_3)_2]^+$ cation, the phenyl and pyridine rings are twisted with respect to the C(10)–C(11)–N(3) plane, having the dihedral angle of 96.6° for the former and 64.5° for the latter. The dihedral angle of the phenyl and pyridine ring is 77.1°. As shown in Fig. 1b, the cations (D) and the anions (A) in **1** stack into a 1D alternating column (i.e., of type ···DDADDADD···) *via* short S(2)···Br(1)(3.681 Å), N(2)···F(1)(3.651 Å), C(14)···N(3)(3.769 Å) interactions, and C(18)–H(18)···Br(1^i) (symmetry code: i = $-x+1$, $-y+1$, $-z+1$) H-bonding interaction with a C(18)···Br(1^i) distance of 3.643 Å. The cation–cation $\pi\cdots\pi$ stacking interactions (the distance between the phenyl rings is 3.552 Å, Fig. 2a) within the above column give further rise to a 2D network structure (Fig. 2b).

The crystal system is changed from triclinic to monoclinic when the Ni(II) ion of **1** is oxidized into Ni(III) ion. An asymmetric unit in a cell of **2** comprises an pair of $[Ni(mnt)_2]^-$ anions and $[FBrBzPyN(CH_3)_2]^+$ cation as shown in Fig. 3a. The selected bond lengths and bond angles are listed in Table 2. The average Ni–S bond distance of 2.147 Å is significantly shorter than that (2.177 Å) of **1**. The coordination geometry of anion and the conformation of cation in **2** are essentially identical to those described above for **1**, and while both anions and cations form segregated

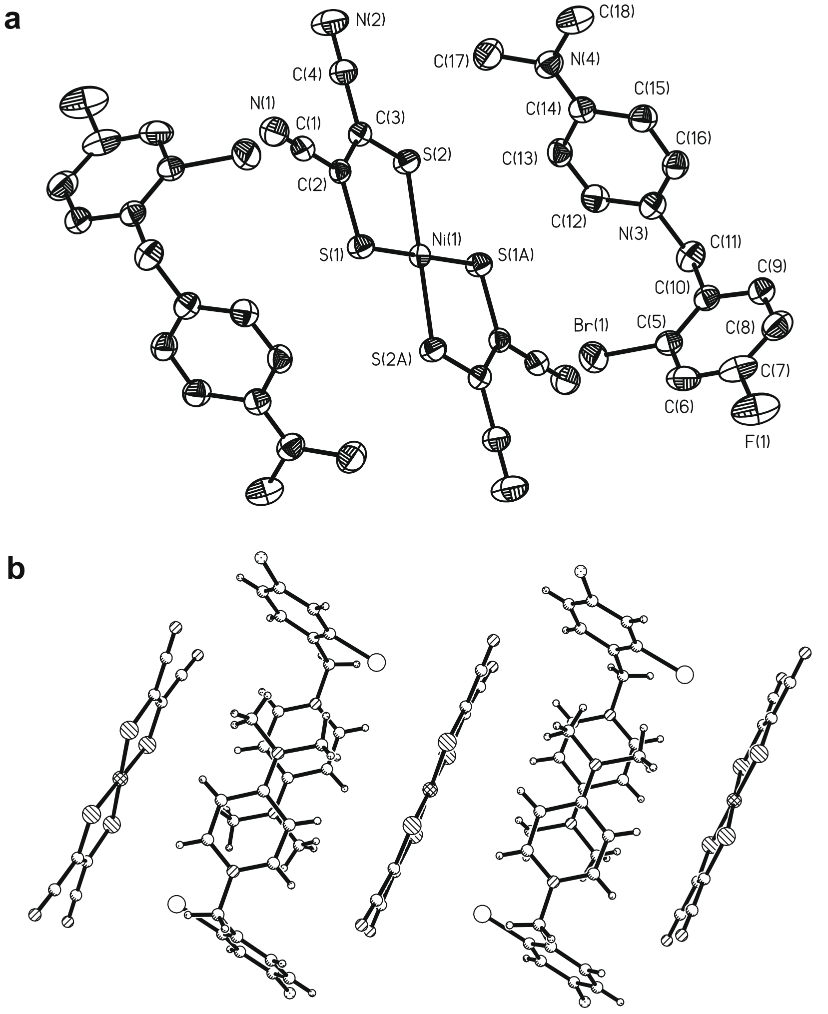

Fig. 1. (a) ORTEP plot (30% probability ellipsoids) showing the molecule structure of **1**. (b) The cations (D) and the anions (A) in **1** stacking into a 1D alternating column (i.e., of type ···DDADDADD···).

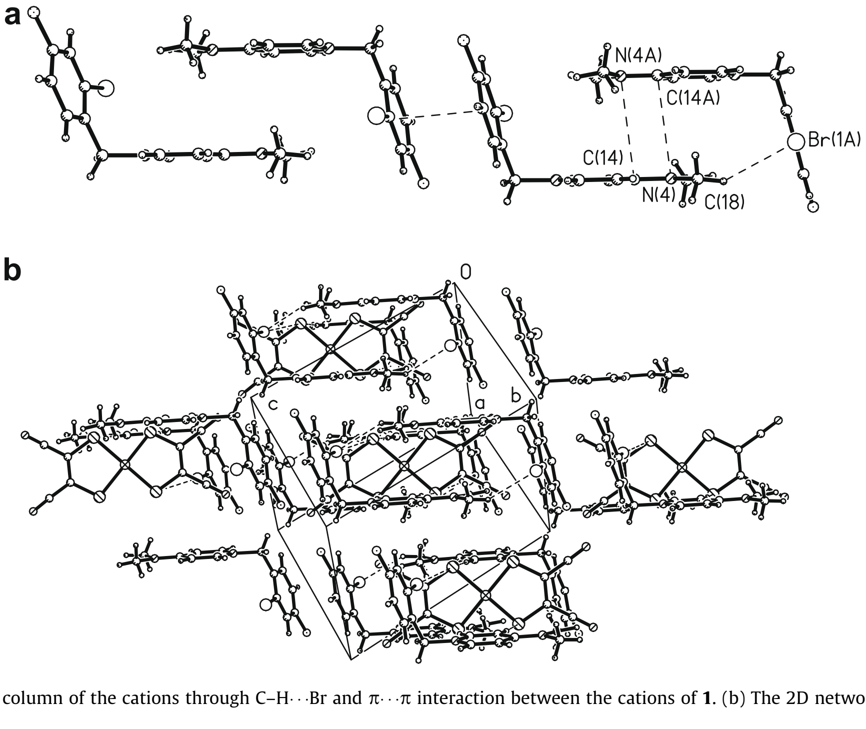

Fig. 2. (a) The 1D column of the cations through C–H···Br and π···π interaction between the cations of **1**. (b) The 2D network structure for **1**.

stacks whose directions do parallel to *a*-axis as shown in Fig. 3b. The most interesting fact is that the four columns of cations create cubic-like large channel in which the $[Ni(mnt)_2]^-$ columns are located (Fig. 3b). The Ni(III) ions form an uniform chain through intermolecular Ni···S, S···S, or Ni···Ni interactions with Ni···Ni distance being 4.024 Å (Fig. 4a). The Ni-ring overlapping mode (Fig. 4b) was found in the pack of $[Ni(mnt)_2]^-$ anions. In the $[FBrBzPyN(CH_3)_2]^+$ cation, the dihedral angles between aromatic ring and the C(14)–C(15)–N(5) plane are 7.8° for the phenyl ring and 86.7° for the pyridine ring. The dihedral angle between the phenyl and pyridine rings is 83.2°. These values are significantly different from those of **1**. The $\pi\cdots\pi$ stacking interactions between the phenyl rings of the neighboring cations with the distance of 3.425 Å give a cations column (Fig. 4c); Besides, two weak H-bonding interactions such as C(10)–H(10)···N(3^{iii}), and C(15)–H(15)···N(4^{iii}) (symmetry code: iii = $-x$, $y-1$, z) are found between the anion and the cation, and the C(10)···N(3), C(15)···N(4) distances are 3.457 Å and 3.285 Å, respectively. These weak cation–cation, anion–anion, and anion–cation interactions in the crystal of **2** generate a 3D network structure (Fig. 3b), and play an important role in the magnetic coupling.

By comparing the structures of **1** and **2**, we conclude that the Ni^{III} ion of the anion favors separated columnar molecular stacks of anions and cations of the crystal when the cation is identical in the two molecular solids. In addition, some short such as S···Br, N···F, C···N interactions, C–H···N, C–H···Br hydrogen bonds, and $\pi\cdots\pi$ stacking interactions play an important role in the stacking and magnetic coupling in the crystal.

3.2. Infrared spectra and UV–Vis spectra

The infrared spectra of **1** and **2** are very much consistent with the structural data presented above. The bands at 3067, 2919, 2853 cm^{-1} for **1** and 3060, 2919, 2846 cm^{-1} for **2** are due to the

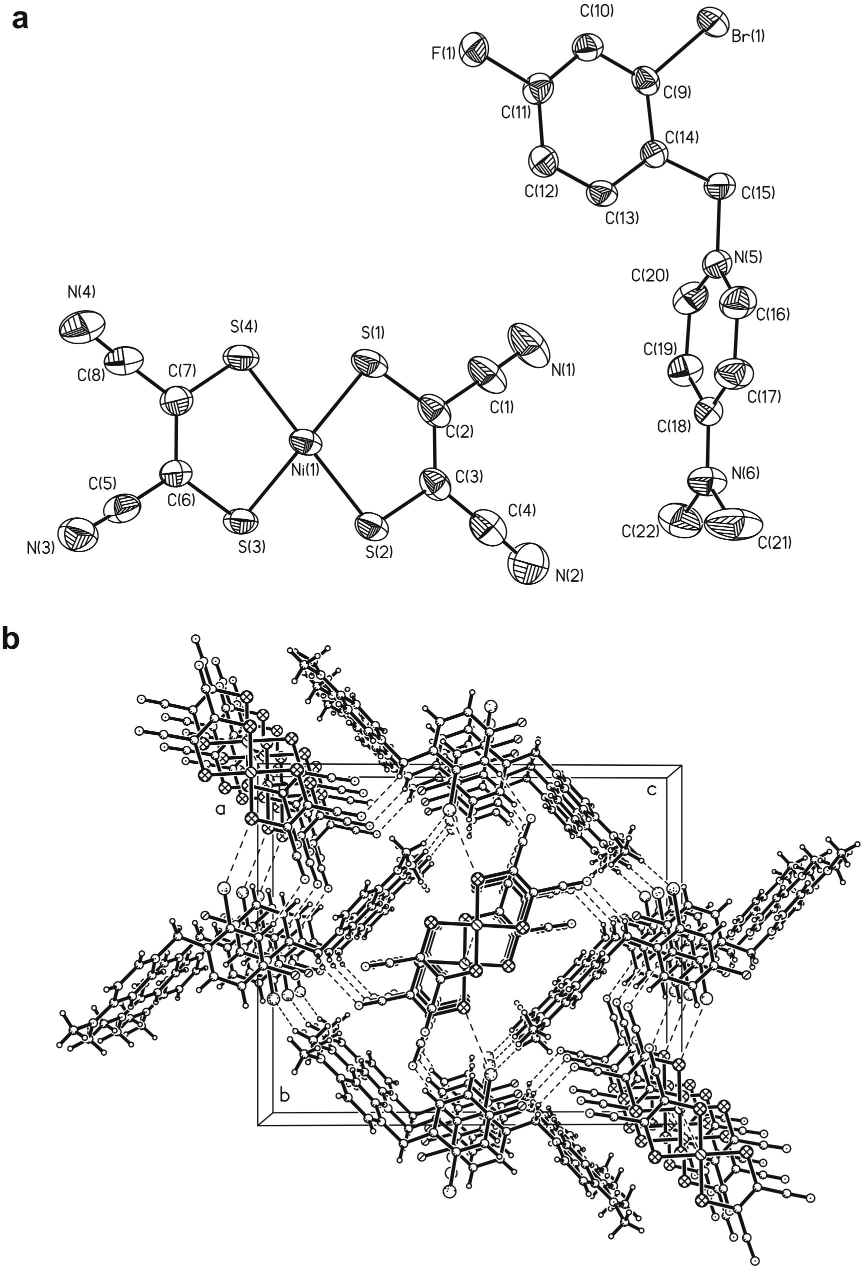

Fig. 3. (a) ORTEP plot (30% probability ellipsoids) showing the molecule structure of **2**. (b) The packing diagram for **2** as viewed along the *a*-axis.

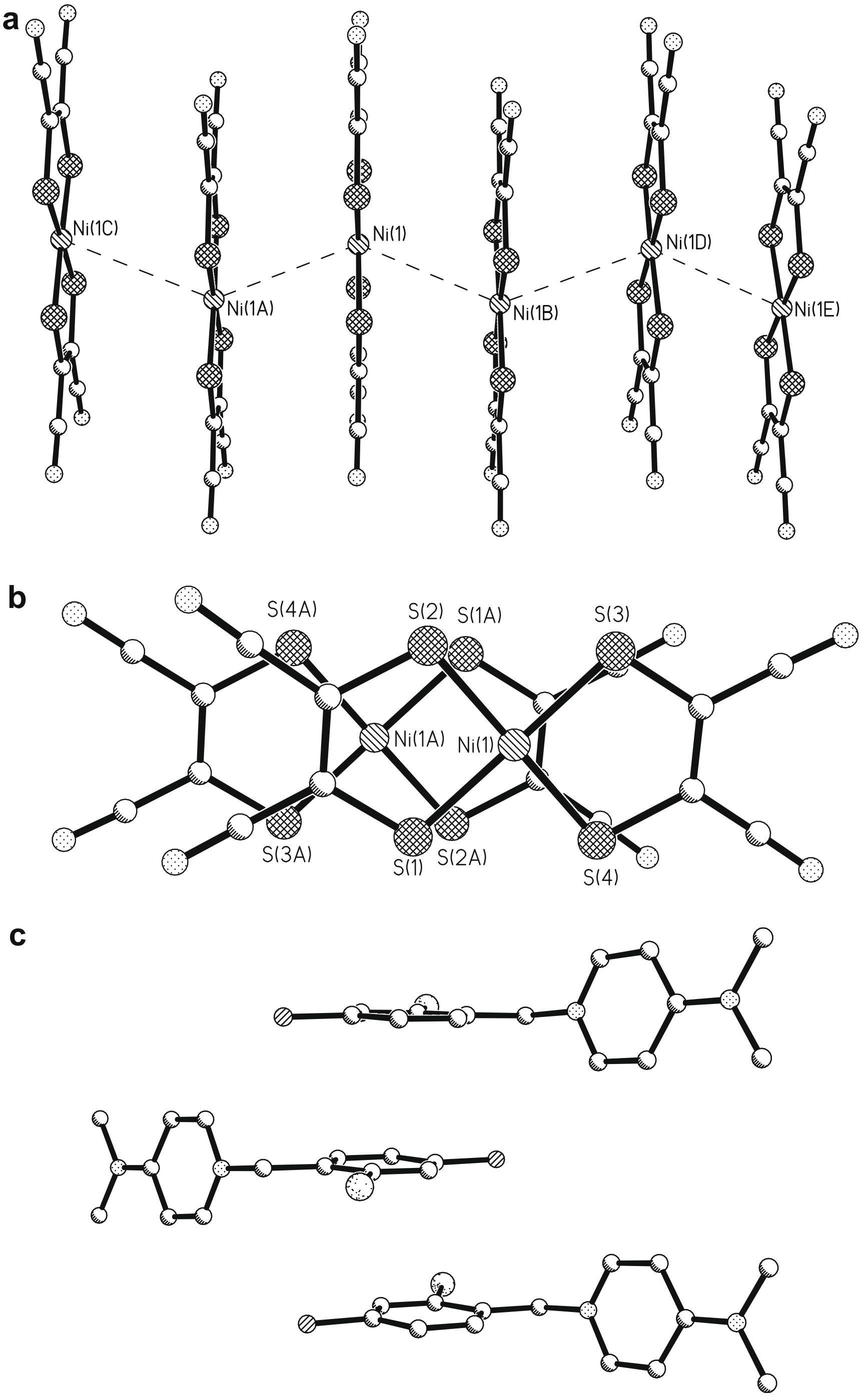

Fig. 4. (a) The Ni(III) ions of $[Ni(mnt)_2]^-$ anions form a 1D zigzag uniform magnetic chain by intermolecular Ni···S, Ni···Ni, or π···π interactions of **2**. (b) Mode of overlapping of the $[Ni(mnt)_2]^-$ anions of **2**. (c) The column of cations via π···π stacking interactions between the phenyl rings for **2**.

stretching vibration frequencies of C–H in the aromatic rings and the methylene. The CN stretching bands lie at 2213, 2195 cm^{-1} for **1** and 2208 cm^{-1} for **2**, respectively, which shows the nickel of **2** is Ni(III) [24]. The bands at 1647, 1596, and 1572 cm^{-1} for **1**, and 1655, 1577, and 1487 cm^{-1} for **2,** are attributable to the C=N and C=C stretching bands for the phenyl and pyridine rings.

The UV–Vis absorption spectra of **1** and **2** in CH_3CN solvent in the region of 200–900 nm are attributed to the anionic portions of these compounds. The characteristic bands of **1** at 878, 472.0, 379, and 272 nm, are assigned as d → d, M → L, L(π) → M, and L(σ) → M, respectively, which is basically similar to those observations in $[Bu_4N]_2[Ni(mnt)_2]$ [25]. The d → d, M → L, L(π) → M, and $L^* \rightarrow L$ bands of **2** are at 864, 474, 376, and 272 nm, respectively, which are similar to these of $[Bu_4N][Ni(mnt)_2]$ [25].

3.3. Magnetic properties and analyses

The magnetic susceptibility data of **2** measured under an applied field of 2000 Oe in the 2–300 K temperature range is shown in Fig. 5, where χ_m is the magnetic susceptibility per nickel atom corrected by the diamagnetic contribution. The overall magnetic behavior of **2** corresponds to a paramagnetic system with an antiferromagnetic coupling interaction. The $\chi_m T$ value at 300 K is only 0.260 emu K mol^{-1} which is significantly lower than the spin-only

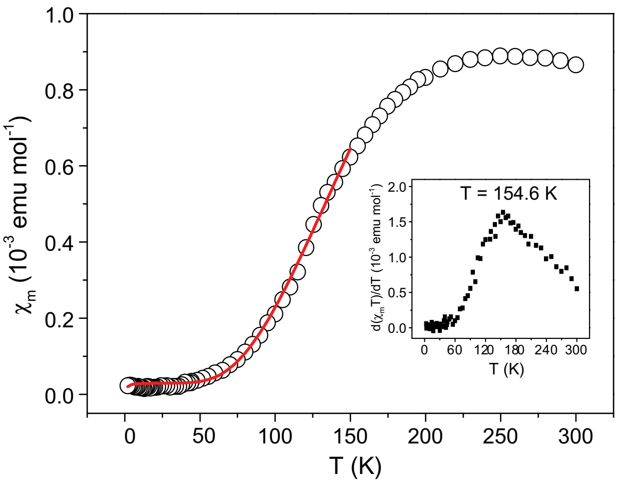

Fig. 5. Plot of χ_m vs. T for **2** (inset: the plot d($\chi_m T$)/dT vs. T) (the red solid lines are reproduced from the theoretic calculations and detailed fitting procedure described in the text). (For interpretation of the references to colour in this figure legend, the reader is referred to the web version of this article.)

value expected for a $s = 1/2$ Ni(III) system (0.375 emu K mol^{-1}). When the temperature decreases, the value of χ_m slightly decreases. While below 155 K, the χ_m values decrease exponentially (Fig. 5), indicating that **2** exhibits the characteristics of a spin gap system [26–29]. On increasing of temperature from 2 K back to 300 K, the same χ_m-T curves are obtained without hysteresis that indicates that **1** undergoes a reversible spin transition. The spin transition temperature is evaluated as the temperature at the maximum of the d($\chi_m T$)/dT derivative, that is, ~155 K for **1** (inset of Fig. 5). The magnetic susceptibility for **2** may be simulated by the formula [30]:

$$\chi_m = \alpha \exp(-\Delta/k_bT)/T + C/T + \chi_0 \tag{1}$$

where α is a constant corresponding to the dispersion of excitation energy, $\varDelta$ is the magnitude of the spin gap, k_b is the Boltzmann constant, C is a constant corresponding to the contribution of the magnetic impurity, χ_0 contributes from the core diamagnetism and the possible Van Vleck paramagnetism. As observed in Fig. 5 (the red solid line), Eq. (1) provides a good fit of experimental data within the range of 2.0–155 K for **2** with $\alpha = 1.99$, $\varDelta/k_b = 460.6$ K, $\chi_0 = 3.0 \times 10^{-5}$ emu mol^{-1}, $C = 2.0 \times 10^{-5}$ emu K mol^{-1}, and $R = 1.1 \times 10^{-6}$ (R is defined as $\Sigma(\chi_{m-}{}^{\text{calcd}}\ \chi_m{}^{\text{obsd}})^2/(\chi_m{}^{\text{obsd}})^2$). The value of the parameter $2\varDelta/k_bTc$ (Tc is the transition temperature) is estimated to be 5.96 for **1**, which is larger than the ideal value of 3.53 derived from the BCS formula in a weak coupling regime. The magnetic coupling between $[\mathrm{Ni(mnt)_2}]^-$ anions is very sensitive to the overlap fashion of neighboring $[\mathrm{Ni(mnt)_2}]^-$ anions and intermolecular contacts [5,31]. On the temperature is lowered, the non-uniform compression of the magnetic chain and slippage of the $[\mathrm{Ni(mnt)_2}]^-$ stack due to the anisotropic contraction of the crystal result in the magnetic exchange constant changing and trigger a spin-gap transition [32].

4. Conclusion

In summary, two new ion-pair complexes, $[\mathrm{FBrBzPyN(CH_3)_2}]_2[\mathrm{Ni(mnt)_2}]$ (**1**) and $[\mathrm{FBrBzPyN(CH_3)_2}][\mathrm{Ni(mnt)_2}]$ (**2**) has been prepared and characterized by single crystal X-ray diffraction and magnetic measurements. Compounds **1** and **2** form a 2D and 3D network structure, respectively. The Ni(III) ions for **2** form a uniform 1D zigzag magnetic chain through Ni···S, Ni···Ni, or π···π interactions with Ni···Ni distance of 4.024 Å. Magnetic susceptibility measurements in the temperature range 2–300 K show that **1** is expected to be diamagnetic, and **2** exhibits an interesting spin-gap transition ($\varDelta/k_b = 460.6$ K) around 155 K.

5. Supplementary material

CCDC 711693 and 711694 contain the supplementary crystallographic data for this paper. These data can be obtained free of charge from the Cambridge Crystallographic Data Center, via http://www.ccdc.cam.ac.uk/data_request/cif.

Acknowledgements

The authors thank the Science and Technology Project (No. 2008B080701011) from Guangdong Science and Technology Department and the President's Science Foundation of South China Agricultural University (No. 2008X015) for financial support of this work.

References

[1] M.E. Itkis, X. Chi, A.W. Corde, R.C. Haddon, Science 296 (2002) 1443.
[2] W. Fujita, K. Awaga, Science 286 (1999) 261.
[3] O. Kahn, C.J. Martinez, Science 297 (1998) 44.
[4] P. Gutlich, Y. Garcia, T. Woike, Coord. Chem. Rev. 219 (2001) 839.
[5] A.T. Coomber, D. Beljonne, R.H. Friend, J.L. Bredas, A. Charlton, N. Robertson, A.E. Underhill, M. Kurmoo, P. Day, Nature 380 (1996) 144.
[6] C.L. Ni, D.Y. Song, Q.J. Meng, Chem. Phys. Lett. 419 (2006) 351.
[7] N. Robertson, L. Cronin, Coord. Chem. Rev. 227 (2002) 93.
[8] J. Nishijo, E. Ogura, J. Yamaura, A. Miyazaki, T. Enoki, T. Takano, Y. Kuwatani, M. Iyoda, Solid State Commun. 116 (2000) 661.
[9] J.L. Xie, X.M. Ren, Y. Song, W.W. Zhang, W.L. Liu, C. He, Q.J. Meng, Chem. Commun. (2002) 2346.
[10] M. Ren, Q.J. Meng, Y. Song, C.L. Lu, C.J. Hu, X.Y. Chen, Z.L. Xue, Inorg. Chem. 41 (2002) 5931.
[11] C.L. Ni, D.B. Dang, Y.Z. Li, S. Gao, Z.P. Ni, Z.F. Tian, Q.J. Meng, J. Solid State Chem. 178 (2005) 100.
[12] X.M. Ren, S. Nishihara, T. Akutagawa, S. Noro, T. Nakamura, W. Fujita, K. Awaga, Chem. Phys. Lett. 418 (2006) 423.
[13] C.L. Ni, J.R. Zhou, Z.F. Tian, Z.P. Ni, Y.Z. Li, Q.J. Meng, Inorg. Chem. Commun. 10 (2007) 880.
[14] C.L. Ni, L.L. Yu, L.M. Yang, Inorg. Chim. Acta 359 (2006) 1383.
[15] C.L. Ni, X.P. Liu, L.L. Yu, L.M. Yang, J. Phys. Chem. Solids 68 (2007) 59.
[16] Y. Hou, C.L. Ni, J.R. Zhou, X.P. Liu, L.L. Yu, L.M. Yang, Synth. Met. 158 (2008) 379.
[17] S.B. Bulgarevich, D.V. Bren, D.Y. Movshovic, P. Finocchiaro, S. Failla, J. Mol. Struct. 317 (1994) 147.
[18] A. Davison, R.H. Holm, Inorg. Synth. 10 (1967) 8.
[19] G.M. Sheldrick, SADABS, Bruker AXS Inc., Madison, Wisconsin, USA, 2004.
[20] Brucker, SMART and SAINT, Bruker AXS Inc., Madison, Wisconsin, USA, 2004.
[21] SHELXTL, Version 5.10. Structure Determination Software Programs, Bruker Analytical X-ray Systems Inc., Madison, Wisconsin, USA, 2000.
[22] C.L. Ni, Y.P. Zheng, L.L. Yang, Y.Z. Li, J. Coord. Chem. 59 (2006) 1037.
[23] S.B. Yang, C.L. Ni, Acta Cryst. E62 (2006) m483.
[24] M.K. Johnson, Vibrational Spectra of Dithiolene Complexes in Dithiolene Chemistry, Progress in Inorganic Chemistry, John Wiley & Sons Inc., New York, 2004.
[25] S.I. Shupack, E. Billig, R.J.H. Clark, R. Williams, H.B. Gray, J. Am. Chem. Soc. 86 (1964) 4594.
[26] C. Yasuda, S. Todo, M. Matsumoto, H. Takayama, J. Phys. Chem. Solids 63 (2002) 1607.
[27] S. Nishihara, T. Akutagawa, T. Hasegawa, T. Nakamura, Chem. Commun. (2002) 408.
[28] S. Nishihara, T. Akutagawa, T. Hasegawa, S. Fujiyama, T. Nakamura, J. Solid State Chem. 168 (2002) 661.
[29] Y. Fujii, T. Goto, W. fujita, K. Awaga, Physica B 329–333 (2003) 973.
[30] L.C. Isett, D.M. Rosso, G.L. Bottger, Phys. Rev. B 22 (1980) 4739.
[31] Z.P. Ni, X.M. Ren, J. Ma, J.L. Xie, C.L. Ni, Z.D. Chen, Q.J. Meng, J. Am. Chem. Soc. 127 (2005) 14330.
[32] X.M. Ren, S. Nishihara, T. Akutagawa, S. Noro, T. Nakamura, W. Fujita, K. Awaga, Z.P. Ni, J.L. Xie, Q.J. Meng, R.K. Kremer, J. Chem. Soc. Dalton Trans. (2006) 1988.